sustainability

MDPI

Article

Oxidative Magnetic Modification of Pristine Biochar Assisted by Ball-Milling for Removal of Methylene Blue and Tetracycline in Aqueous Solution

Yijia Chen [1,2], Linzhou Li [1,2], Qin Wen [1,2], Run Yang [1,2], Yiming Zhao [1,2], Xin Rao [1,2], Jihui Li [1,2,3,*], Shuying Xu [1,2] and Hui Song [1,2]

[1] Key Laboratory of Ministry of Education for Advanced Materials in Tropical Island Resources, School of Chemical Engineering and Technology, Hainan University, Haikou 570228, China; yjceeaa@163.com (Y.C.); hndxzch1998@163.com (L.L.); wenqin_hg@hainanu.edu.cn (Q.W.); yangrun0703@163.com (R.Y.); zhaoyiming1998@163.com (Y.Z.); raoxin_hg@163.com (X.R.); xushuying1980@hainanu.edu.cn (S.X.); songhui@hainanu.edu.cn (H.S.)

[2] Key Laboratory of Solid Waste Resource Utilization and Environmental Protection, Hainan University, Haikou 570228, China

[3] School of Science, Hainan University, Haikou 570228, China

* Correspondence: lijihui@hainanu.edu.cn

Abstract: Magnetic modification holds a significant place for regulating the performance of biochar for wastewater treatment, endowing its magnetic separation property and facilitating its wide application. Herein, a ball-milled oxidative magnetic modification of pristine biochar was employed to manufacture magnetic biochar using K_2FeO_4 as a precursor and internal oxidant for removal of methylene blue and tetracycline from aqueous solution. The characterizations showed that magnetic iron oxide and oxygen-containing groups were simultaneously introduced. Moreover, specific surface area and pore volume were remarkably enhanced from 0.7 m^2/g to 71.2 m^2/g and from 0.001 cm^3/g to 0.034 cm^3/g, respectively. The magnetic biochar showed that 133.76 mg/g and 58.34 mg/g adsorption capacities for MB and TC, respectively, significantly transcended the pristine biochar. Its adsorption was mainly dominated by oxygen-containing groups and iron species. This would provide an efficient oxidative magnetic modification for the preparation of oxygen-containing group-rich magnetic biochar for the removal of MB and TC.

Keywords: ball-milling; oxidative magnetic modification; magnetic biochar; methylene blue; tetracycline

Citation: Chen, Y.; Li, L.; Wen, Q.; Yang, R.; Zhao, Y.; Rao, X.; Li, J.; Xu, S.; Song, H. Oxidative Magnetic Modification of Pristine Biochar Assisted by Ball-Milling for Removal of Methylene Blue and Tetracycline in Aqueous Solution. *Sustainability* **2022**, *14*, 9349. https://doi.org/10.3390/su14159349

Academic Editor: Salvatore Cataldo

Received: 31 May 2022
Accepted: 22 July 2022
Published: 30 July 2022

1. Introduction

Biochar has captured widespread attention as a low-cost carbon-based material for environmental remediation with unique characteristics and tunable structure [1,2]. In particular, magnetic biochar finds wide applications for removing pollutants from wastewater with intriguing magnetic separation property [3,4]. Generally, magnetic biochar is manufactured by impregnating magnetic media such as iron, nickel, and cobalt species into a biochar matrix through either pyrolysis or post-treatment [5]. Magnetic iron species, for instance, zerovalent iron, Fe_3O_4, and γ-Fe_2O_3, are prevailing candidates owing to their low-cost and environmental friendliness.

Usually, zerovalent iron doped biochar is manufactured via the reduction of biochar loaded with iron oxides by $NaBH_4$ (This can be called "reductive magnetic modification") [6]. By contrast, iron oxide doped magnetic biochar is air-stable and thereby has great potential for industrial application. This kind of biochar can be prepared by doping magnetic iron oxide via either co-pyrolysis or base-induced co-precipitation using ferric and ferrous as precursors [5]. However, high pyrolysis temperature is used for gaining either magnetic iron oxide medium or biochar matrix with a large specific surface area for loading iron species in most cases, easily causing loss of functional groups on the surface.

They dominate multiple physiochemical properties of carbon matrix, including surface electronegativity, acidic-basic properties, ion exchange, and complexation capability for adsorption, and also serve as active sites for immobilizing iron species.

To expand the application of iron oxide doped magnetic biochar, several modifications were developed to improve its performance in recent years. For instance, functionalization was applied to improve the performance of magnetic biochar using ammonia [7] and iminodiacetic acid [8] for the removal of Cr (VI) and Cd (II), respectively. $CaCO_3$-impregnation was utilized to enhance the adsorption capability of magnetic biochar for As (III) and Cd (II) [9]. Similarly, calcium-based magnetic biochar was also prepared for efficiently adsorbing other heavy metals (Pb (II), Cu (II), and Cr (VI)) using calcium-rich feedstock such as iron sludge [10] and crayfish shell [11]. Chitosan-crosslink was also developed to engineer magnetic biochar for the removal of various heavy metals [12], where the multiple functional groups of chitosan played an important role in the adsorption. This endeavor was mostly dedicated to removing heavy metals and less paid for organic pollutants by now.

Ball-milling is an emerging technology for regulating the physicochemical properties of biochar with several intriguing advantages such as high efficiency and environmentally friendliness [13]. It could improve the physical properties, including specific surface area and pore volume [14], leading to an increased adsorption capability. A great advance has been made in improving adsorption capability of biochar for removing various pollutants using ball-milling in the past decade [15]. Especially, it was applied to modify magnetic biochar for adsorbing heavy metals [16,17], antibiotics [18,19], and dye [20] from an aqueous solution, where multiple physicochemical properties were improved and enhanced adsorption capabilities were achieved.

This work was dedicated to investigating ball-milled K_2FeO_4 modification for the preparation of oxygen-containing group-rich magnetic biochar. To avoid decomposition of oxygen-containing groups during pyrolysis with K_2FeO_4, direct K_2FeO_4 oxidation of pristine biochar was used instead; meanwhile, ball-milling was applied to accelerate this oxidation. It was hoped that additional oxygen functional groups could be simultaneously introduced with magnetic iron species such as Fe_3O_4 and γ-Fe_2O_3 due to the strong oxidizing ability of K_2FeO_4. Meanwhile, ball-milling could accelerate K_2FeO_4 oxidation to boost oxygen-containing groups and improve the physicochemical properties of biochar, such as surface morphology and porous structure. Mangosteen shell, a largely available biowaste mainly consisting of crude fiber and pectin from the tropical fruit mangosteen [21], was used as feedstock to prepare the biochar. The biochar was prepared at a relatively low temperature (300 °C) for conserving functional groups, which was beneficial to K_2FeO_4 oxidation for boosting active oxygen groups such as –COOH and –OH. Such oxidative magnetic modification would provide an efficient method for addressing the shortcoming of the above-mentioned magnetic modifications in a small amount of surface functional groups that were usually achieved. Additionally, the adsorption capabilities of pristine and magnetic biochars toward methylene blue (MB) and tetracycline (TC) were also assessed in an aqueous solution. In short, it was aimed to establish a facile and efficient oxidative magnetic modification for the preparation of highly adsorptive magnetic biochar at low pyrolysis temperature.

2. Material and Methods

2.1. Materials and Feedstock

Mangosteen shell was collected from a fruit market in the Hainan University of Hainan Province in China and used as feedstock. Analytically pure chemicals such as MB, tetracycline hydrochloride, and K_2FeO_4 were purchased from Shanghai Aladdin and Macklin Biochemical Technology Co., Ltd.s. (Shanghai, China) and used without purification.

2.2. Biochar Preparation and Characterization

Mangosteen shell was washed with tap water, dried at 60 °C, and broken into powder (60 mesh). Pristine biochar (PB) was prepared through direct pyrolysis of mangosteen shell at 300 °C for 1 h, washed with ultrapure water, and dried at 60 °C. PB was mixed with K_2FeO_4 and 10 mL ultrapure water (pH = 5), where 2 g PB and 3 g K_2FeO_4 were employed to reduce the formation of aggregates of iron oxides. Then, the mixture was milled with 100 g ball beads (3 mm) on a planetary ball mill (Pulverisette 6, Fritsch GmbH, Germany) at a rotation speed of 400 r/min for 30 min. The ball-milling was paused for 20 min every 10 min to prevent an increase in temperature. The resulted product was washed with ultrapure water until colorless and dried at 60 °C to get oxidized magnetic biochar (OMB).

The organic element contents, including C, H, O, and N, were determined on a Thermo Scientific Flash 2000 CHNS/O analyzer (Waltham, MA, USA) directly. The inorganic elements Fe and K were measured using an inductively coupled plasma atomic-emission spectrometer (Agilent ICPOES730, Palo Alto, CA, USA). The carbon matrix was digested to measure Fe and K content by the mixture of nitric acid, hydrofluoric acid, hydrogen peroxide, and hydrochloric acid in an oven at 180 °C for 8 h. Surface properties were measured using N_2 adsorption/desorption isotherms on an ASAP 2460 analyzer (Micromeritics, Norcross, GA, USA); the specific surface area was determined by Brunauer–Emmett–Teller (BET) model, the pore size and volume were calculated by Barret–Joyner–Halenda (BJH) model. Functional groups were determined by Fourier transform infrared spectrum (FTIR) on a Bruker Tensor 27 infrared spectrometer (Ettlingen, Germany). Surface elements and functional groups were analyzed by X-ray photoelectron spectrum on a Thermo Scientific Escalab 250Xi spectrometer (Waltham, MA, USA). Crystal morphology was analyzed by an X-ray powder diffractometer (Rigaku MiniFlex600, Tokyo, Japan) with Cu Kα radiation from 10–90°. The Zeta potential was measured by a Malvern Zetasizer NANO ZS analyzer (Malvern, UK), where the test was repeated three times, and the average value was reported. The surface structure and element composition analysis was carried out on a scanning electron microscope (Phenom ProX, South Holland, Holland). The chemical structure was also analyzed by Raman spectrum (Renishaw PLC, Gloucestershire, UK) at the wavelength of 514 nm.

2.3. Batch Adsorption Experiments

All the adsorptions were performed using a 1/2 g/L ratio of biochar to adsorbate solution on a shaker at 180 r/min and 25 °C. The concentration of adsorbate was measured before and after adsorption to determine the adsorption capability of biochar. MB concentration was tested by a UV-visible spectrophotometer (MAPADA UV-3300PC, Shanghai, China) at 665 nm, and TC concentration was measured on a high-performance liquid chromatograph (HPLC: Waters e2695, Milford, MA, USA) using a mixture of methanol, acetonitrile, and 0.01 M aqueous oxalic acid solution (8/20/72 volume ratio) as mobile phase. The adsorption experiments were repeated three times, and the adsorption data were presented as mean values with standard deviations. The pHs (3, 5, and 7) were used to evaluate the effect of initial pH of adsorbate solution. The adsorption kinetics were performed at pH = 5, where 100 mg/L and 0.5 mg/L were used for MB, and 100 mg/L and 1 mg/L were applied for TC. For adsorption isotherms, the adsorption was carried out at pH = 5 for 72 h. A series of concentrations including 50 mg/L, 100 mg/L, 150 mg/L, 200 mg/L, 250 mg/L, and 300 mg/L were used to investigate the adsorption of PB for MB and TC, and 25 mg/L, 100 mg/L, 150 mg/L, 200 mg/L, 250 mg/L, 300 mg/L, and 350 mg/L were applied for evaluating the adsorption of OMB toward TC; 100 mg/L, 200 mg/L, 250 mg/L, 300 mg/L, 350 mg/L, 400 mg/L, and 450 mg/L were employed to assess its adsorption toward MB. Co-existed ions including NaCl, $MgCl_2$, $CaCl_2$, $NaNO_3$, Na_2SO_4, Na_3PO_4, and Na_2CO_3 were investigated to evaluate their influence on the adsorption capability of OMB at a high concentration (50 mM). To evaluate the competitive adsorption between MB and TC, the adsorption of OMB was performed in an aqueous mixture solution of them.

2.4. Recycle of Magnetic Biochar

The OMB loaded with MB was regenerated in various solvents, including aqueous HCl (0.1 M), ethanol, acetonitrile, and a mixture of ethanol/acetic acid (9/1 *v/v*) with a 1/2 mg/mL ratio at room temperature for 12 h. TC was desorbed by Fenton oxidation using dilute aqueous H_2O_2 solution (0.03 wt%), where OMB loaded with TC was added to the H_2O_2 solution in 1/2 mg/mL ratio and shaken at room temperature for 12 h.

2.5. Fixed Bed Column Adsorption

Briefly, 250 mg biochar was filled into a plastic column with 10 mm diameter, and the height of OMB and PB was about 6 mm and 9 mm, correspondingly. Pollutant solution was injected into the biochar-filled column from bottom to top with a flow speed of 5.0 mL/min, and the effluent was collected at one-minute interval and measured its concentration. The adsorption cures were depicted as adsorption efficiency (C_t/C_0) versus flow time (T).

3. Results and Discussion

3.1. Biochar Characterization

As listed in Table 1, a large amount of Fe was impregnated into OMB, and higher oxygen content was achieved for OMB than PB. Therefore, K_2FeO_4 succeeded in oxidizing the biochar matrix to produce iron oxides and oxygen-containing groups with the assistance of ball-milling. Moreover, much higher content of K was observed on OMB than PB, meaning that it was also introduced using K_2FeO_4 as precursor. Importantly, much larger specific surface area (SSA) and pore volume (PV) were achieved for OMB than PB. Pore diameter (PD) decreased sharply from 60.0 nm to 3.0 nm because of iron oxide filling and pore collapse. This suggested the combination of K_2FeO_4 oxidation and ball-milling induced a synergistic effect for regulating multiple physicochemical properties of biochar.

Table 1. The physicochemical properties of biochars.

BC	Element Content (wt%)						Surface Properties		
	C	H	O	N	Fe	K	SSA (m^2/g)	PV (cm^3/g)	PD (nm)
PB	63.2	4.3	24.6	0.6	0.0	1.4	0.7	0.001	60.0
OMB	30.7	2.9	31.8	0.3	24.1	2.8	71.2	0.034	3.0

SEM images showed that wrinkle and compact surface was observed for PB, yet a smooth surface was achieved for OMB due to K_2FeO_4 oxidation (Figure 1a–d). Moreover, a certain amount of pores were observed on OMB, leading to a larger PV (Table 1). EDS spectra indicated that C, O, and K were found on the surface of PB (Figure 1e–h). C, O, K, and Fe were coated on the surface of OMB with sheet structure (Figure 1i–m). Meanwhile, OMB possessed much higher relative oxygen content (17.91/31.22 vs. 30.16/65.64) than PB, which was consistent with elemental analysis. Additionally, K was introduced onto the surface of OMB. It is worth mentioning that it should exist in the form of –COOK and –OK, and thereby higher cation exchange capacity was achieved for OMB.

The crystalline of biochar was analyzed by XRD spectra (Figure 2a). A broad peak around 21.46°, which could be assigned to cellulose I [22], was observed on PB but was hardly detected on OMB without the peaks of crystal carbon. This suggested crystal cellulose was converted into an amorphous carbon structure with ball-milled K_2FeO_4 modification [23]. Additionally, three peaks around 35.38°, 44.82°, and 62.58° were found on OMB.

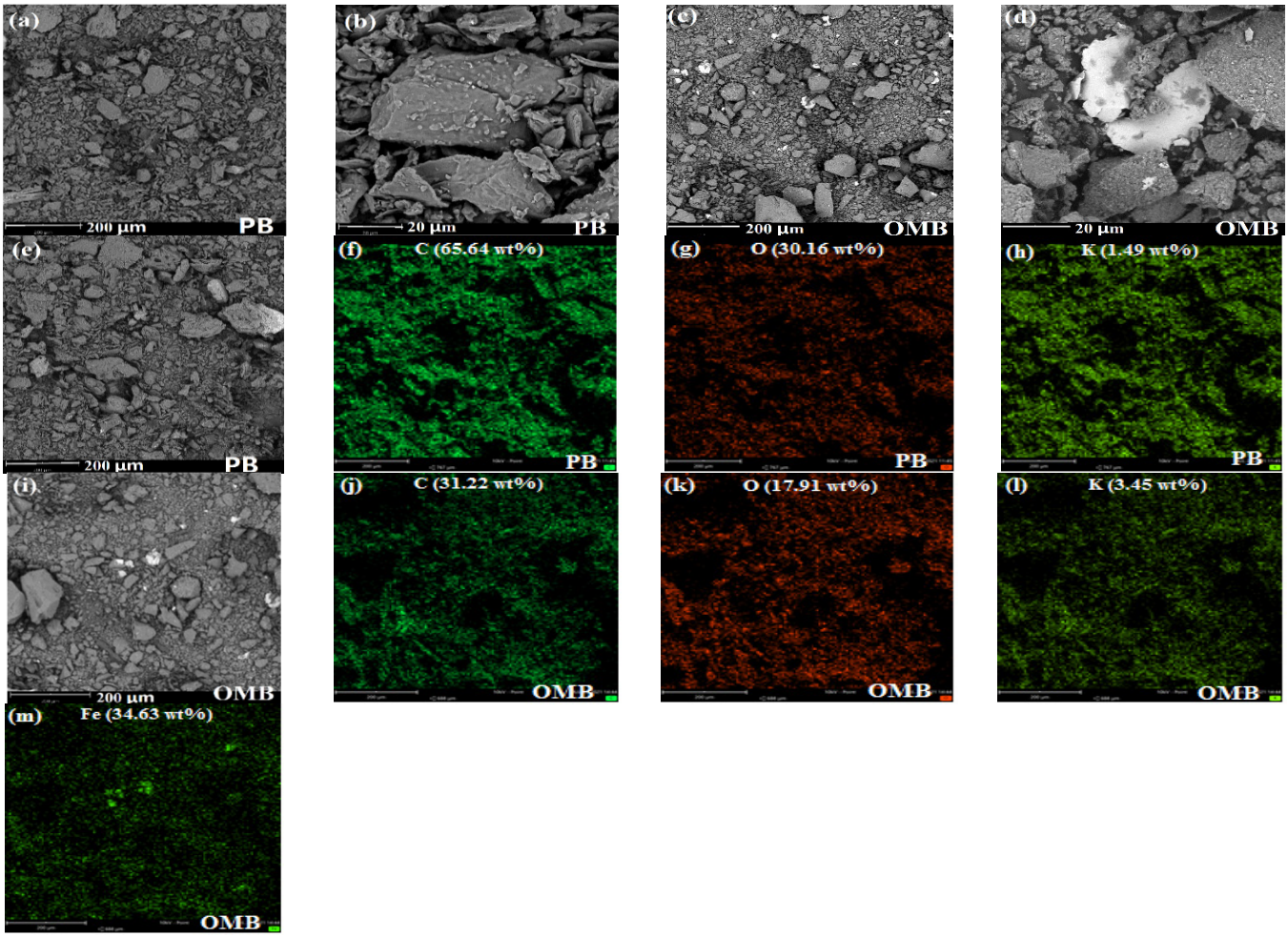

Figure 1. SEM images (**a**–**d**) and EDS spectra (**e**–**m**) of biochars.

These peaks could be attributed to either Fe_3O_4 or γ-Fe_2O_3, endowing OMB 10.22 emu/g saturation magnetization (SM) (Figure 2b). Raman spectra were performed to distinguish these magnetic iron species. Two peaks around 1323 cm^{-1} and 1583 cm^{-1}, assigned to G and D bands of carbon correspondingly, were achieved for both biochars. Additionally, four peaks at 215 cm^{-1}, 274 cm^{-1}, 382 cm^{-1}, and 690 cm^{-1} were detected on OMB (Figure 2c). They should be attributed to Fe-O vibration of Fe_3O_4 and Fe-C vibration on the surface of OMB [24]. Therefore, the magnetic iron medium doped on OMB should mostly be Fe_3O_4. It should be noted that amorphous iron oxides were also impregnated besides Fe_3O_4. This was verified by the fact that OMB had a much lower SM than the calculated one [25] based on the 24.1% content of iron (Table 1).

The FTIR spectra showed that several functional groups, including –OH (3452 cm^{-1}), aliphatic C-H (2833 cm^{-1}, 1392 cm^{-1}), C=O/C=C (1645 cm^{-1}), and C-O (1110 cm^{-1}) groups were generated on the biochars (Figure 2d). OMB possessed comparable intensity of these peaks as PB even though iron oxides were introduced. Moreover, aromatic C-H (777 cm^{-1}) was also observed on them [26]. Compared to PB, OMB had higher aromaticity as a stronger peak of aromatic C-H was observed. It could be concluded that ball-milled K_2FeO_4 oxidation facilitated the formation of oxygen-containing groups and aromatic structures through oxidation and dehydration, respectively. Apparently, a higher negative potential was observed for OMB than PB (Figure 2e) due to the introduction of oxygen-containing groups and iron oxides on the surface [27]. OMB still displayed electronegativity at strong acidic condition (pH = 3). Such a high negatively charged surface will be beneficial to adsorb cationic pollutants by electrostatic interaction.

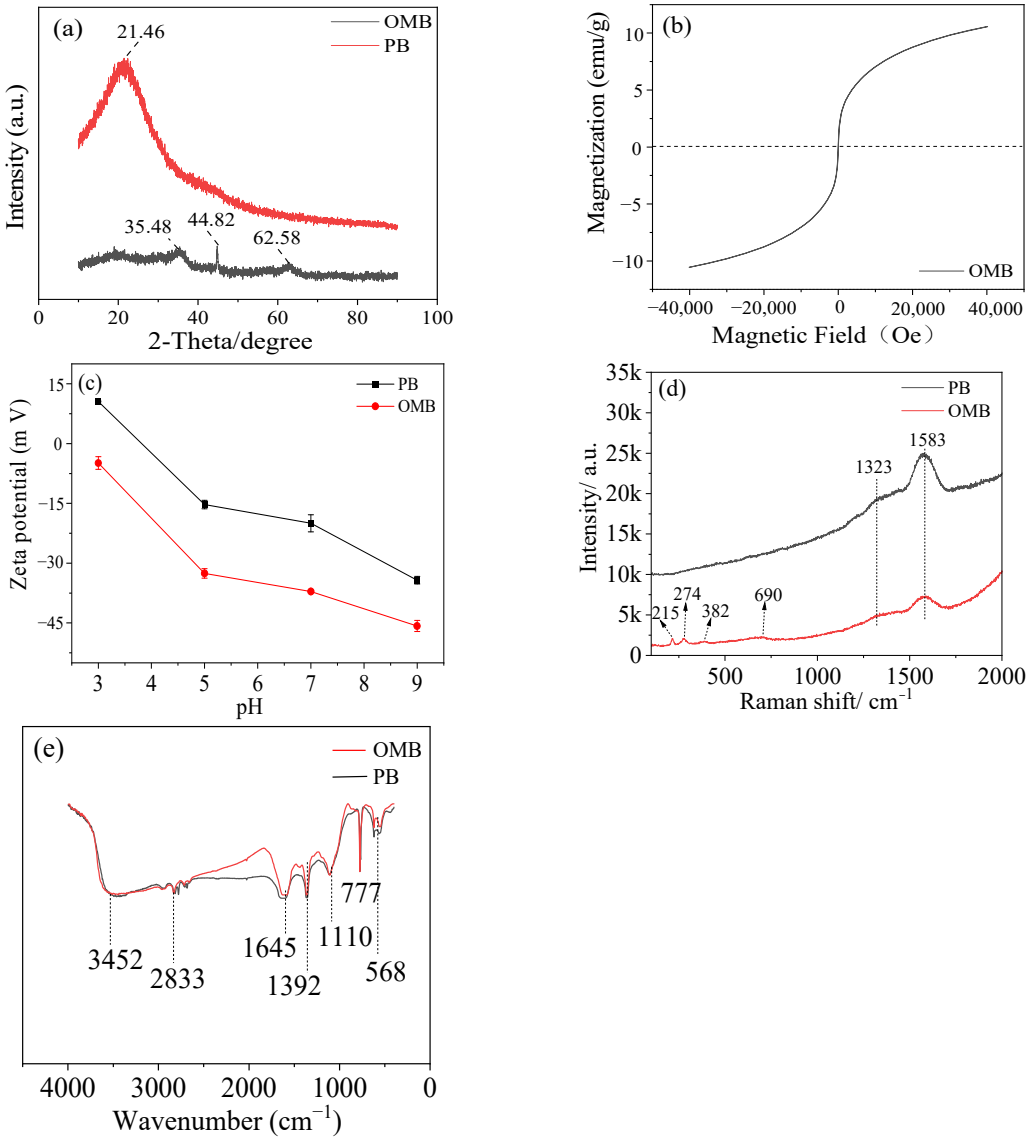

Figure 2. Characterization of biochars by XRD pattern (**a**), hysteresis curve (**b**), Zeta potential (**c**), Raman spectra (**d**), and FTIR (**e**).

PB and OMB were mainly composed of C/O/N and C/O/N/Fe/K on their surfaces correspondingly (Figure 3a,b). The high-resolution C1s spectra indicated that PB primarily consisted of C-C/C=C (284.8 eV), C-OH (286.3 eV), and C-O-C (287.1 eV) groups [28,29] (Figure 3c). Importantly, C=O (288.6 eV) was also detected on OMB besides these peaks (Figure 3d). Evidently, OMB had much higher content of all these oxygen-containing groups than PB, indicating that K_2FeO_4 oxidation efficiently oxidized the carbon matrix and produced new oxygen-containing groups on its surface, where ball milling should also play an important role in the acceleration of K_2FeO_4 oxidation as well as regulation of surface structure. O1s spectra revealed that O-C and O=C were obtained on PB with H_2O [30,31] (Figure 3e). Besides these groups, Fe-O-Fe and Fe-OH were also generated on OMB [30,32] (Figure 3f), and thereby iron hydroxides and iron oxides were simultaneously incorporated. The high-resolution Fe 2P spectrum indicated that Fe^{2+} and Fe^{3+} were observed in the ratio of 0.85/1 (Figure 3g). A pair of peaks at 710.4 eV and 723.9 eV with a satellite peak at 714.9 eV were detected, which were assigned to Fe^{2+} [33,34]. Likewise, a pair of peaks at 712.3 eV and 726.3 eV with a satellite peak of 719.1 eV were observed for Fe^{3+}. In summary, new oxygen-containing groups were generated on the carbon matrix, and ferric/ferrous oxides and hydroxides were impregnated by using K_2FeO_4 as a precursor.

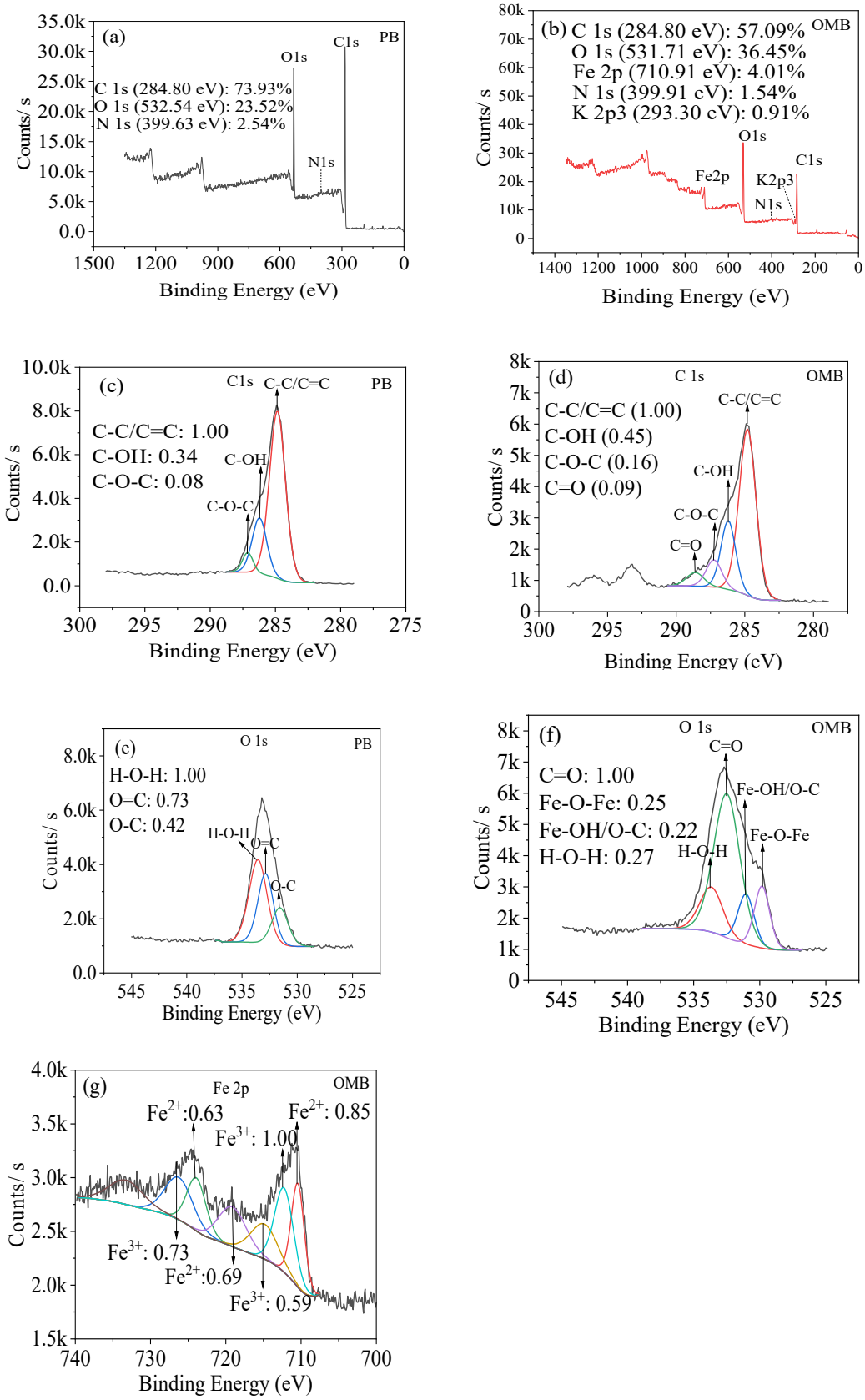

Figure 3. XPS spectra ((**a**,**b**): survey spectra, (**c**,**d**): C 1s spectra, (**e**,**f**): O 1s spectra, (**g**): Fe 2p spectrum.) of biochars.

3.2. Adsorption Capability of Biochar for MB and TC

3.2.1. The Effect of Initial pH

The adsorption capability of PB was maintained at a low level for both MB and TC over a pH range of 3–7 (Figure 4a,b); even increased zeta potential was obtained with pH (Figure 2e), implying electrostatic interaction wasn't a dominating factor. The adsorption of OMB toward MB greatly increased from 78.51 mg/g to 170.56 mg/g, enhancing the initial pH from 3 to 5 (Figure 4a). The increase in Zeta potential and reduction of H^+ exchange against MB cation might be the main reasons for causing this phenomenon. While higher pH was employed, the adsorption almost remained at this level. Interestingly, its adsorption toward TC was less influenced by initial pH, and good adsorption capability was gained (Figure 4b). This suggested that OMB showed good compatibility for adsorption of variable TC as a different state of TC was formed at these pHs [35]. Therefore, it was a powerful adsorbent for the removal of TC in different pH aqueous environments. Significantly, OMB always displayed much higher adsorption capabilities toward MB and TC than PB over a wide pH range.

3.2.2. Adsorption Kinetics and Isotherms

As shown in Figure 4c,d, OMB processed much higher adsorption speed and equilibrium adsorption capabilities for MB and TC at a high concentration (100 mg/L). OMB could rapidly remove most MB at low concentration (0.5 mg/L) within 10 min, even using 1/8 g/L biochar dosage (Figure 4e), and most TC (1 mg/L) within 10 h (Figure 4f). By contrast, PB only adsorbed 70% of MB and 43% of TC at the above-mentioned concentrations (Figure 4f,g). Moreover, OMB also could adsorb most MB at a wide range of low concentrations (1–5 mg/L) but showed a lower removal ratio for TC (Figure 4h). These adsorption data were closely described by pseudo second model (see Supplementary Materials), suggesting that these adsorptions were chemically controlled processes.

The adsorption isotherms are depicted in Figure 4i,j; PB showed low adsorption capacities for both MB (3.69 mg/g) and TC (7.86 mg/g). In the case of OMB, much higher adsorption capacities (MB: 133.76 mg/g, TC: 58.34 mg/g) were gained, indicating that ball-milling accelerated K_2FeO_4 oxidation could efficiently enhance the adsorption capability of mangosteen shell biochar. The enhancement of adsorption capability could be attributed to the introduction of oxygen-containing groups and iron oxides, as well as the enlargement of SSA and PV. Their adsorptions were accurately described by the Freundlich model ($R^2 > 0.95$) (see Supplementary Materials) and should be multilayer heterogeneous adsorption processes [29]. The Freundlich exponents n were greater than 1, suggesting they were favorable processes [36,37]. Higher values of n were obtained for OMB than PB. Therefore, ball-milled K_2FeO_4 oxidation not only endowed the biochar good magnetic response but also improved its adsorption efficiency. This would provide an efficient and low energy consumption method for the preparation of magnetic biochar for efficient removal of MB and TC compared to the existed methods (Table 2). It should be pointed out that the adsorption capability and magnetism of the magnetic biochar could be further improved by using a longer ball milling time and a higher ratio of K_2FeO_4 to pristine biochar.

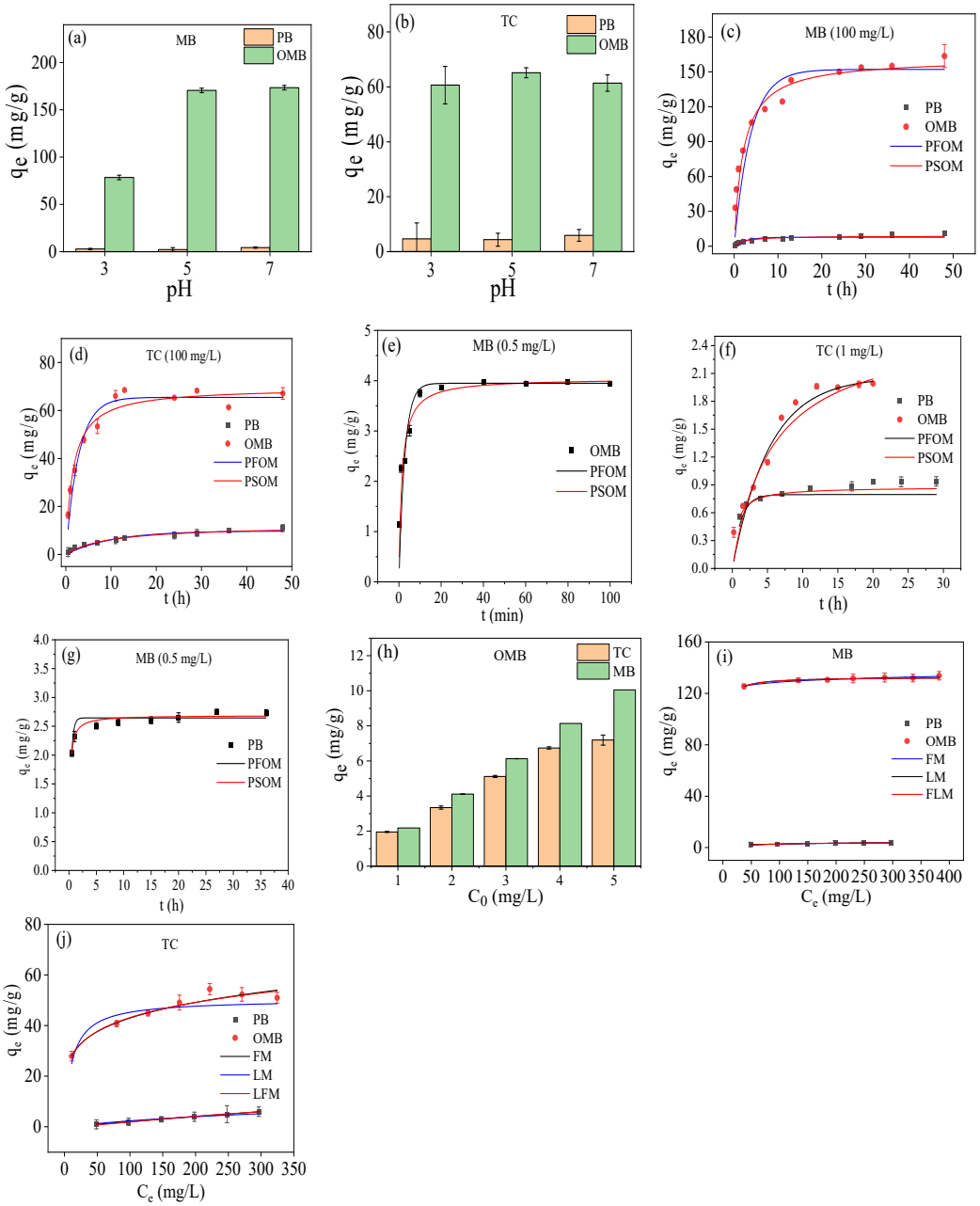

Figure 4. The effect of initial pH (**a**,**b**): 100 mg/L, 1/2 g/L, 25 °C; adsorption kinetics at high concentration (**c**,**d**): 1/2 g/L, pH = 5, 25 °C and low concentration (**e**,**f**) (MB): 1/8 g/L, pH = 5, 25 °C; (**g**) (TC): 1/2 g/L, pH = 5, 25 °C; adsorption isotherms (**h**,**i**): 1/2 g/L, pH = 5, 25 °C; adsorption capability of OMB at different low concentrations (**j**): 1/2 g/L, pH = 5, 25 °C, 48 h.

Table 2. Summary of preparation methods of magnetic biochar for removal of MB and TC.

Magnetic Biochar	Preparation Method	Q_m (mg/g)	SM (emu/g)	Ref.
Fe_3O_4-doped biochar	Hydrothermal carbonation with iron mud at 180 °C for 12 h	186.003 (MB)	22.35	[38]
Fe_3O_4-doped biochar	Co-pyrolysis with Fe_3O_4 at 500 °C for 30 min	52.6 (MB)	—	[39]
Fe_2O_3-doped biochar	Pretreatment by Fe_2O_3/$KMnO_4$/HNO_3 and pyrolysis at 800 °C for 20 min	46.30 (MB)	—	[40]
Fe_3O_4-doped biochar	Pyrolysis at 600 °C for 4 h and ball-mill extrusion with Fe_3O_4 for 12 h	500.5 (MB)	34.9	[20]
Fe_3O_4-doped biochar	$KMnO_4$-activation, pyrolysis at 500 °C for 2 h, and base-induced co-precipitation	98.89 (TC)	64.7	[41]
Fe_3O_4-doped biochar	Pyrolysis at 700 °C for 3 h and base-induced co-precipitation	42.31 (TC)	26.28	[42]
Fe_3O_4-doped biochar	Iron impregnation, pyrolysis at 700 °C for 2 h, and ball-milling for 12 h	268.3 (TC)	15.39	[16]
Fe_3O_4-doped biochar	Base promoted hydrothermal carbonization at 230 °C for 24 h and heat treatment at 400 °C for 1 h	48.35 (TC)	9.73	[43]
Fe_3O_4-doped biochar	Microwave-assisted pyrolysis at 700 °C for 2 h and microwave hydrothermal treatment with iron at 200 °C for 1 h	202.62 (TC)	—	[44]
γ-Fe_2O_3 doped biochar	Pyrolysis at 800 °C for 2 h and alkali-acid modification	286.913 (TC)	—	[45]
Fe_3O_4-doped biochar	Pyrolysis at 300 °C for 1 h, and ball-milling with K_2FeO_4 for 30 min	133.76 (MB), 58.34 (TC)	10.22	This work

3.2.3. Effect of Co-Existed Mineral on the Adsorption of Magnetic Biochar

Co-existing minerals might interact with biochar and adsorbate in an aqueous solution and influence their adsorption behavior greatly. The effect of common minerals such as NaCl, $MgCl_2$, $CaCl_2$, $NaNO_3$, Na_2SO_4, Na_2CO_3, and Na_3PO_4 was investigated at a high concentration (50 mM) (Figure 5a,b). The adsorption of OMB was disturbed by these minerals for MB (Figure 5a) due to the competitive adsorption of metal cation against MB cation by ion exchange. A similar phenomenon was also found for its adsorption toward TC (Figure 5b), which should be resulted from the reduction of active adsorption sites as anion could occupy oxygen-containing groups and ion center by hydrogen bonding and complexation correspondingly. The "squeeze-out effect" of minerals could also be one reason for the decrease in its adsorption [46,47]. In comparison to Na^+, the bivalent cations Mg^{2+} and Ca^{2+} caused a sharp decrease in adsorption capability for MB and TC owing to the occupation of oxygen-containing groups by their stronger complexation. Moreover, they might exchange with K^+ and weaken electronegativity and cation exchange capability, resulting in a decrease in MB adsorption. Oxygen anions SO_4^{2-}, PO_4^{3-}, and CO_3^{2-} also heavily disturbed the adsorption of MB on account of their occupation of the active Fe center and hydrogen (−COOH and −OH) by complexation and hydrogen bondings. By contrast, these anions slightly disturbed the adsorption of TC as they could bridge it with OMB by $-NH_2$ and –OH groups. Additionally, OMB exhibited displayed good and moderate adsorption capabilities for MB and TC in domestic wastewater, respectively. Thus, OMB should be a potential adsorbent for the removal of MB and TC in industrial wastewater.

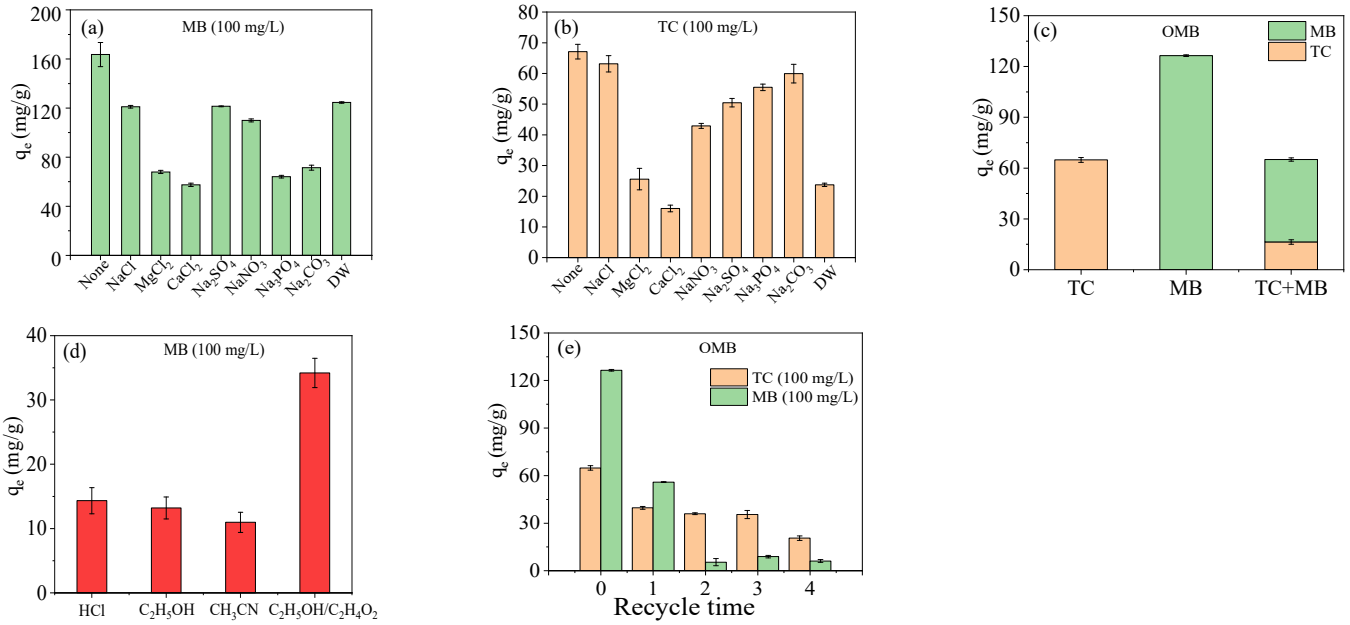

Figure 5. Effect of co-existed mineral (**a**,**b**): 1/2 g/L, pH = 5, 25 °C, 48 h; the adsorption capability in the mixture solution of MB and TC (**c**): 100 mg/L MB + 100 mg/L TC, 1/2 g/L, pH = 5, 0.25 °C; recycle of OMB (**d**,**e**): pH = 5, 25 °C, 24 h.

3.2.4. Competitive Adsorption Behavior of MB and TC

The adsorption behavior of OMB was also evaluated in the binary system of MB (Figure 5c). The adsorption of MB and TC decreased simultaneously as limited active adsorption sites participated in the adsorption of either MB or TC. Even though MB ($C_{16}H_{18}N_3ClS$ (319.85 g/mol)) had a lower molecular weight than TC ($C_{22}H_{24}N_2O_8$•HCl (480.90 g/mol)), its adsorption was still much higher than that of TC, probably because of its additional cation exchange with OMB. This was consistent with the adsorption result in single solutions of MB and TC. Thus, the cation exchange of MB was less influenced by TC, probably owing to the stronger exchangeability of –COOK and -OK on OMB.

3.2.5. Recycle of Magnetic Biochar

To recycle OMB, different regenerants were employed to desorb MB and TC. MB was desorbed in several solvents, including aqueous HCl (0.1 M), ethanol, acetonitrile, and a mixture of ethanol and acetic acid (9/1 *v/v*). The regeneration was the best in the mixture of ethanol and acetic acid and led to the decrease in adsorption capability for MB from 126.45 mg/g to 55.93 mg/g for the first time (Figure 5d). Low adsorption capability was achieved after the first recycle. Fenton oxidative degradation was investigated to desorb TC using a low concentration of H_2O_2 (0.03%). The first regeneration resulted in the reduction of adsorption capability from 64.86 mg/g to 39.68 mg/g (Figure 5e), and the adsorption capability diminished to 20.60 mg/g after four times recycle.

3.2.6. Fixed Bed Column Adsorption

To further assess the industrial applicability of the biochars, a continuous adsorption study was carried out. The breakthrough curves of PB and OMB are depicted in Figure 6. For PB, the adsorption ratio of MB gradually decreased with sampling time at a concentration of 25 mg/L, whereas that of TC decreased rapidly at a relatively low concentration (10 mg/L). A similar result was also achieved for the adsorption of them at high concentrations (MB: 500 mg/L, TC: 150 mg/L) by OMB. The adsorption data could be suitably simulated by Thomas and Yoon-Nelson models [10,35] (see Supplementary Materials). The maximum adsorption capacities of OMB calculated by the Thomas model were much larger than that of PB. Compared to PB, OMB had longer and comparable breakthrough times (t_b)

of 50% (C_t/C_0 = 0.5) for MB (1.97 min vs. 0.88 min) and TC (0.39 vs. 0.38) even at higher concentrations, indicating that ball-milled K_2FeO_4 could efficiently improve the adsorption capability of mangosteen shell biochar for industrial application.

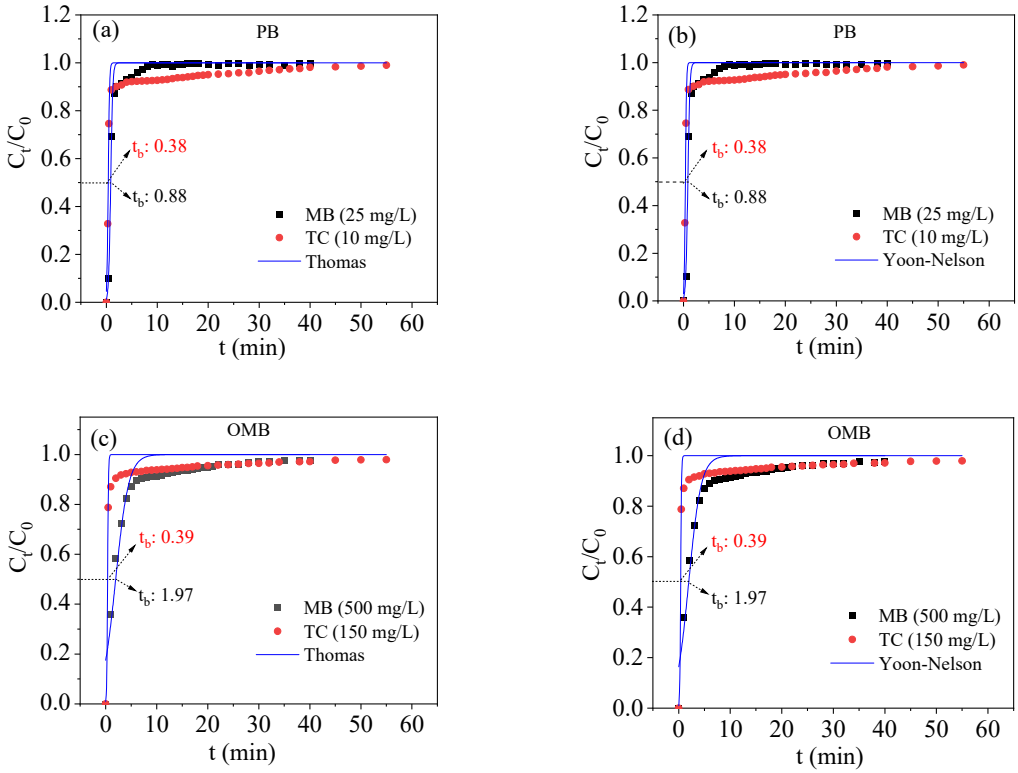

Figure 6. Fixed column adsorption curves ((**a**,**b**): PB, (**c**,**d**): OMB.) of biochars (pH = 5, 25 °C).

3.2.7. Adsorption Mechanism of OMB

As TC primarily existed in the form of electrically neutral molecule $TC^{\pm}$ at pH = 5 [35], electrostatic interaction should be ruled out in its adsorption. OMB and TC were rich in functional containing groups (including C=O, C-O-C, –OH, and $–NH_2$), so they could interact with each other through hydrogen bonding. Moreover, hydrogen bonding and coordination of TC with iron oxides and hydroxides should be involved in the adsorption. For MB, hydrogen bonding and complexation of N on MB with hydroxyl and iron of OMB should be involved in the adsorption. Cation exchange and electrostatic interaction could also participate in the adsorption of MB as a certain amount of COOK and –OK were observed, and a negatively charged surface was obtained for OMB. Additionally, a high aromatic structure was generated on OMB, so π–π electrostatic interaction should be involved in its adsorption for MB and TC. Therefore, carbon matrix and iron species simultaneously contributed to the adsorption of OMB toward MB and TC.

4. Conclusions

Ball-milling assisted K_2FeO_4 modification succeeded in efficiently oxidizing pristine biochar and impregnating magnetic γ-Fe_2O_3 within a short time. Various oxygen-containing groups such as –OH, C=O, and C-O-C were introduced with nonmagnetic iron oxides; meanwhile, the specific surface area and pore volume were significantly enhanced. The magnetic biochar displayed much higher adsorption capacities for MB and TC than the pristine biochar with good saturation magnetization. It can also efficiently remove them at low concentrations from an aqueous solution. Oxygen-containing groups and iron species collaborated with each other for their adsorption. This would provide an efficient and low energy-consumed approach to preparing magnetic biochar for the removal of MB and TC in an aqueous solution.

Supplementary Materials: The following supporting information can be downloaded at: https://www.mdpi.com/article/10.3390/su14159349/s1, Table S1: The fitted parameters of adsorption kinetics; Table S2: The fitted parameters of adsorption isotherms; Table S3. The fitted parameters of fixed bed column adsorption.

Author Contributions: Conceptualization, J.L.; methodology, Y.C. and J.L.; software, Y.C. and L.L.; validation, L.L., Q.W. and R.Y.; formal analysis, J.L. and S.X.; investigation, Y.C., L.L. and Y.Z.; resources, J.L. and H.S.; data curation, Q.W. and X.R.; writing—original draft preparation, Y.C.; writing—review and editing, J.L.; visualization, Y.C.; supervision, J.L.; project administration, J.L., S.X. and H.S.; funding acquisition, J.L. All authors have read and agreed to the published version of the manuscript.

Funding: This research was funded by the National Natural Science Foundation of China [52160018, 21801053] and the Hainan Provincial Natural Science Foundation of China [422RC600, 519QN175] for funding this research. The APC was funded by the Hainan Provincial Natural Science Foundation of China [422RC600, 519QN175].

Institutional Review Board Statement: Not applicable.

Informed Consent Statement: Not applicable.

Data Availability Statement: Not applicable.

Acknowledgments: Special thanks to the reviewers for their valuable comments.

Conflicts of Interest: The authors declare no conflict of interest.

References

1. Panahi, H.S.K.; Dehhaghi, M.; Yong, S.O.; Nizami, A.S.; Khoshnevisan, B.; Mussatto, S.I.; Aghbashlo, M.; Tabatabaei, M.; Lam, S.S. A comprehensive review of engineered biochar: Production, characteristics, and environmental applications. *J. Clean. Prod.* **2020**, *270*, 122462. [CrossRef]
2. Zhou, Y.; Qin, S.; Verma, S.; Sar, T.; Sarsaiya, S.; Ravindran, B.; Liu, T.; Sindhu, R.; Patel, A.K.; Binod, P.; et al. Production and beneficial impact of biochar for environmental application: A comprehensive review. *Bioresour. Technol.* **2020**, *337*, 125451. [CrossRef] [PubMed]
3. Li, X.; Wang, C.; Zhang, J.; Liu, J.; Liu, B.; Chen, G. Preparation and application of magnetic biochar in water treatment: A critical review. *Sci. Total Environ.* **2020**, *711*, 134847. [CrossRef]
4. Rocha, L.S.; Pereira, D.; Sousa, E.; Otero, M.; Esteves, V.I.; Calisto, V. Recent advances on the development and application of magnetic activated carbon and char for the removal of pharmaceutical compounds from waters: A review. *Sci. Total Environ.* **2020**, *718*, 137272. [CrossRef] [PubMed]
5. Yi, Y.; Huang, Z.; Lu, B.; Xian, J.; Tsang, E.P.; Cheng, W.; Fang, J.; Fang, Z. Magnetic biochar for environmental remediation: A review. *Bioresour. Technol.* **2020**, *298*, 122468. [CrossRef] [PubMed]
6. Wang, S.; Zhao, M.; Zhou, M.; Li, Y.C.; Wang, J.; Gao, B.; Sato, S.; Feng, K.; Yin, W.; Igalavithana, A.D.; et al. Biochar-supported nZVI (nZVI/BC) for contaminant removal from soil and water: A critical review. *J. Hazard. Mater.* **2019**, *373*, 820–834. [CrossRef]
7. Mian, M.M.; Liu, G.; Yousaf, B.; Fu, B.; Ullah, H.; Ali, M.U.; Abbas, Q.; Mujtaba, M.A.M.; Ruijia, L. Simultaneous functionalization and magnetization of biochar via NH_3 ambiance pyrolysis for efficient removal of Cr (VI). *Chemosphere* **2018**, *208*, 712–721. [CrossRef] [PubMed]
8. Zhou, X.; Zhou, J.; Liu, Y.; Guo, J.; Ren, J.; Zhou, F. Preparation of iminodiacetic acid-modified magnetic biochar by carbonization, magnetization and functional modification for Cd (II) removal in water. *Fuel* **2018**, *233*, 469–479. [CrossRef]
9. Wu, J.; Huang, D.; Liu, X.; Meng, J.; Tang, C.; Xu, J. Remediation of As (III) and Cd (II) co-contamination and its mechanism in aqueous systems by a novel calcium-based magnetic biochar. *J. Hazard. Mater.* **2018**, *348*, 10–19. [CrossRef] [PubMed]
10. Wang, S.; Bian, S.; Liu, J.; Li, J.; Xu, S.; Liang, Z. Highly adsorptive pristine and magnetic biochars prepared from crayfish shell for removal of Cu (II) and Pb (II). *J. Taiwan Inst. Chem. Eng.* **2021**, *127*, 175–185. [CrossRef]
11. Duan, S.; Ma, W.; Pan, Y.; Meng, F.; Yu, S.; Wu, L. Synthesis of magnetic biochar from iron sludge for the enhancement of Cr (VI) removal from solution. *J. Taiwan Inst. Chem. Eng.* **2017**, *80*, 835–841. [CrossRef]
12. Chin, J.F.; Heng, Z.W.; Teoh, H.C.; Chong, W.C.; Pang, Y.L. Recent development of magnetic biochar crosslinked chitosan on heavy metal removal from wastewater—Modification, application and mechanism. *Chemosphere* **2021**, *291*, 133035. [CrossRef] [PubMed]
13. Kumar, M.; Xiong, X.; Wan, Z.; Sun, Y.; Tsang, D.; Gupta, J.; Gao, B.; Cao, X.; Tang, J.; Yong, S.O. Ball milling as a mechanochemmical technology for fabrication of novel biochar nanomaterials. *J. Bioresour. Technol.* **2020**, *312*, 123613. [CrossRef] [PubMed]
14. Amusat, S.O.; Kebede, T.G.; Dube, S.; Nindi, M.M. Ball-milling synthesis of biochar and biochar–based nanocomposites and prospects for removal of emerging contaminants: A review. *J. Water Process Eng.* **2021**, *41*, 101993. [CrossRef]

15. Lyu, H.; Gao, B.; He, F.; Zimmerman, A.R.; Ding, C.; Huang, H.; Tang, J. Effects of ball milling on the physicochemical and sorptive properties of biochar: Experimental observations and governing mechanisms. *Environ. Pollut.* **2018**, *233*, 54–63. [CrossRef]
16. Li, R.; Zhang, Y.; Deng, H.; Zhang, Z.; Wang, J.J.; Shaheen, S.M.; Xiao, R.; Rinklebe, J.; Xi, B.; He, X.; et al. Removing tetracycline and Hg(II) with ball-milled magnetic nanobiochar and its potential on polluted irrigation water reclamation. *J. Hazard. Mater.* **2020**, *384*, 121095. [CrossRef] [PubMed]
17. Zou, H.; Zhao, J.; He, F.; Zhong, Z.; Huang, J.; Zheng, Y.; Zhang, Y.; Yang, Y.; Yu, F.; Bashir, M.A.; et al. Ball milling biochar iron oxide composites for the removal of chromium (Cr (VI)) from water: Performance and mechanisms. *J. Hazard. Mater.* **2021**, *413*, 125252. [CrossRef]
18. Huang, J.; Zimmerman, A.R.; Chen, H.; Gao, B. Ball milled biochar effectively removes sulfamethoxazole and sulfapyridine antibiotics from water and wastewater. *Environ. Pollut.* **2020**, *258*, 113809. [CrossRef]
19. Shan, D.; Deng, S.; Zhao, T.; Wang, B.; Wang, Y.; Huang, J.; Yu, G.; Winglee, J.; Wiesner, M.R. Preparation of ultrafine magnetic biochar and activated carbon for pharmaceutical adsorption and subsequent degradation by ball milling. *J. Hazard. Mater.* **2016**, *305*, 156–163. [CrossRef]
20. Li, Y.; Zimmerman, A.R.; He, F.; Chen, J.; Han, L.; Chen, H.; Hu, X.; Gao, B. Solvent-free synthesis of magnetic biochar and activated carbon through ball-mill extrusion with Fe_3O_4 nanoparticles for enhancing adsorption of methylene blue. *Sci. Total Environ.* **2020**, *722*, 137972. [CrossRef]
21. Anitha, D.; Ramadevi, A.; Seetharaman, R. Biosorptive removal of Nickel(II) from aqueous solution by Mangosteen shell activated carbon. *Mater. Today Proceed.* **2021**, *45*, 718–722. [CrossRef]
22. Wen, Q.; Wang, S.; Liu, S.; Li, J.; Chen, Y.; Yang, R.; Xu, S. Investigation of seawater mineral promoted pyrolysis at low temperature for improving the adsorption capabilities of biochar. *Chemosphere* **2021**, *292*, 133447. [CrossRef] [PubMed]
23. Zhou, X.; Moghaddam, B.T.; Chen, M.; Wu, S.; Adhikari, S. Biochar removes volatile organic compounds generated from asphalt. *Sci. Total. Environ.* **2020**, *745*, 141096. [CrossRef]
24. Nguyen, H.V.; Van, T.H.; Nguyen, Q.V.; Dam, V.X.; Hoang, P.L.; Ha, T.L. Magnetic Fe_3O_4 nanoparticle biochar derived from pomelo peel for reactive red 21 adsorption from aqueous solution. *J. Chem.* **2020**, *2020*, 3080612. [CrossRef]
25. Liu, Y.; Wang, Y.; Zhou, S.; Lou, S.; Yuan, L.; Gao, T.; Wu, X.; Shi, X.; Wang, K. Synthesis of high saturation magnetization superparamagnetic Fe3O4 hollow microspheres for swift chromium removal. *ACS Appl. Mater. Inter.* **2012**, *4*, 4913–4920. [CrossRef] [PubMed]
26. Özçimen, D.; Ersoy-Meriçboyu, A. Characterization of biochar and bio-oil samples obtained from carbonization of various biomass materials. *Renew. Energ.* **2010**, *35*, 1319–1324. [CrossRef]
27. Zhang, P.; O'Connor, D.; Wang, Y.; Jiang, L.; Xia, T.; Wang, L.; Tsang, D.C.W.; Yong, S.O.; Hou, D. A green biochar/iron oxide composite for methylene blue removal. *J. Hazard. Mater.* **2020**, *384*, 121286. [CrossRef] [PubMed]
28. Akhavan, O.; Ghaderi, E.; Emamy, H.; Akhavan, F. Genotoxicity of graphene nanoribbons in human mesenchymal stem cells. *Carbon* **2013**, *54*, 419–431. [CrossRef]
29. Peng, H.; Gao, P.; Chu, G.; Pan, B.; Peng, J.; Xing, B. Enhanced adsorption of Cu (II) and Cd (II) by phosphoric acid-modified biochars. *Environ. Pollut.* **2017**, *229*, 846–853. [CrossRef]
30. Ahmed, M.B.; Zhou, J.L.; Ngo, H.H.; Johir, M.A.H.; Sornalingam, K. Sorptive removal of phenolic endocrine disruptors by functionalized biochar: Competitive interaction mechanism, removal efficacy and application in wastewater. *Chem. Eng. J.* **2018**, *335*, 801–811. [CrossRef]
31. Yang, Z.; Qian, K.; Lv, J.; Yan, W.; Liu, J.; Ai, J.; Zhang, Y.; Guo, T.; Zhou, X.; Xu, S.; et al. Encapsulation of Fe_3O_4 nanoparticles into N, S co-doped graphene sheets with greatly enhanced electrochemical performance. *Sci. Rep.* **2016**, *6*, 27957. [CrossRef]
32. Yang, F.; Zhang, S.; Li, H.; Li, S.; Cheng, K.; Li, J.-S.; Tsang, D.C.W. Corn straw-derived biochar impregnated with α-FeOOH nanorods for highly effective copper removal. *Chem. Eng. J.* **2018**, *348*, 191–201. [CrossRef]
33. Yamashita, T.; Hayes, P. Analysis of XPS spectra of Fe^{2+} and Fe^{3+} ions in oxide materials. *App. Surf. Sci.* **2008**, *254*, 2441–2449. [CrossRef]
34. Zhang, P.; Hou, D.; Li, X.; Pehkonen, S.; Varma, R.S.; Wang, X. Greener and size-specific synthesis of stable Fe-Cu oxides as earth-abundant adsorbents for malachite green. *J. Mater. Chem. A* **2018**, *6*, 9229–9236.
35. Zhang, X.; Li, Y.; Wu, M.; Pang, Y.; Hao, Z.; Hu, M.; Qiu, R.; Chen, Z. Enhanced adsorption of tetracycline by an iron and manganese oxides loaded biochar: Kinetics, mechanism and column adsorption. *Bioresour. Technol.* **2021**, *320*, 124264. [CrossRef]
36. Fan, S.; Wang, Y.; Wang, Z.; Tang, J.; Tang, J.; Li, X. Removal of methylene blue from aqueous solution by sewage sludge-derived biochar: Adsorption kinetics, equilibrium, thermodynamics and mechanism. *J. Environ. Chem. Eng.* **2017**, *5*, 601–611. [CrossRef]
37. Hameed, B.H.; Ahmad, A.A.; Aziz, N. Isotherms, kinetics and thermodynamics of acid dye adsorption on activated palm ash. *Chem. Eng. J.* **2007**, *133*, 195–203. [CrossRef]
38. Zeng, H.; Qi, W.; Zhai, L.; Wang, F.; Zhang, J.; Li, D. Magnetic biochar synthesized with waterworks sludge and sewage sludge and its potential for methylene blue removal. *J. Environ. Chem. Eng.* **2021**, *9*, 105951. [CrossRef]
39. Cho, D.W.; Lee, J.; Yong, S.O.; Kwon, E.E.; Song, H. Fabrication of a novel magnetic carbon nanocomposite adsorbent via pyrolysis of sugar. *Chemosphere* **2016**, *163*, 305–312. [CrossRef] [PubMed]
40. Ruthiraan, M.; Abdullah, E.C.; Mubarak, N.M.; Noraini, M.N. A promising route of magnetic based materials for removal of cadmium and methylene blue from waste water. *J. Environ. Chem. Eng.* **2017**, *5*, 1447–1455. [CrossRef]

41. Oladipo, A.A.; Ifebajo, A.O. Highly efficient magnetic chicken bone biochar for removal of tetracycline and fluorescent dye from wastewater: Two-stage adsorber analysis. *J. Environ. Manag.* **2018**, *209*, 9–16. [CrossRef] [PubMed]
42. Yao, X.; Ji, L.; Guo, J.; Ge, S.; Lu, W.; Cai, L.; Wang, Y.; Song, W.; Zhang, H. Magnetic activated biochar nanocomposites derived from wakame and its application in methylene blue adsorption. *Bioresour. Technol.* **2020**, *302*, 122842. [CrossRef]
43. Rattanachueskul, N.; Saning, A.; Kaowphong, S.; Chumha, N.; Chuenchom, L. Magnetic carbon composites with a hierarchical structure for adsorption of tetracycline, prepared from sugarcane bagasse via hydrothermal carbonization coupled with simple heat treatment process. *Bioresour. Technol.* **2017**, *226*, 164–172. [CrossRef]
44. Qu, J.; Wang, S.; Jin, L.; Liu, Y.; Yin, R.; Jiang, Z.; Tao, Y.; Huang, J.; Zhang, Y. Magnetic porous biochar with high specific surface area derived from microwave-assisted hydrothermal and pyrolysis treatments of water hyacinth for Cr (VI) and tetracycline adsorption from water. *Bioresour. Technol.* **2021**, *340*, 125692. [CrossRef]
45. Tang, L.; Yu, J.; Pang, Y.; Zeng, G.; Deng, Y.; Wang, J.; Ren, X.; Ye, S.; Peng, B.; Feng, H. Sustainable efficient adsorbent: Alkali-acid modified magnetic biochar derived from sewage sludge for aqueous organic contaminant removal. *Chem. Eng. J.* **2018**, *336*, 160–169. [CrossRef]
46. Wei, X.; Zhang, R.; Zhang, W.; Yuan, Y.; Lai, B. High-efficiency adsorption of tetracycline by the prepared waste collagen fiber-derived porous biochar. *RSC Adv.* **2019**, *9*, 39355–39366. [CrossRef] [PubMed]
47. Zhou, Y.; Apul, O.G.; Karanfil, T. Adsorption of halogenated aliphatic contaminants by graphene nanomaterials. *Water Res.* **2015**, *79*, 57–67. [CrossRef] [PubMed]